APPLICATIONS OF IMAGE RECONSTRUCTION IN NDE

R.V. Denton and S. Maitra
Systems Control, Inc.
Palo Alto, CA 94304

ABSTRACT

The nondestructive evaluation (NDE) of materials often involves the solution of an inverse problem. It is shown that image reconstruction techniques lead to the direct solution of the 3-D inverse problem when radiographic measurements are made. In particular, it is suggested that the convolve-and-backproject solution to the 3-D divergent ray geometry problem should be useful for NDE. There is also a discussion of the accept-reject criteria appropriate for various classes of defects.

INTRODUCTION

There has been a strong emphasis on defect characterization through ultrasonic scattering measurements in the previous ARPA/AFML Progress Reviews [1]. Here the ultimate goal is to invert the scattering data, i.e., to solve the inverse problem, in order to arrive at quantitative estimates of the three-dimensional size, the shape, and the orientation of defects. This problem can be solved for the case of fairly simple defects that are situated in structures of uncomplicated geometries. However, this inverse problem becomes extremely difficult to solve for complex structures, due to the many possible internal reflections which can occur. In an industrial setting, it is the many internal reflections, together with refraction and diffraction phenomena, which lead to ambiguities in identifying defects when using ultrasonic measurements.

It is for this reason that radiographic measurements, whenever applicable, will always play an important role in nondestructive evaluation (NDE). The geometric optics limit is applicable in radiographic techniques; the wavelength of the X-rays or of the emitted radiation from radioisotopes is much smaller than the size of the scatterers. The rays travel in straight-line paths between scattering events, and a typical transmission measurement simply determines the net scattering out of the beam direction.

Radiographic transmission measurements, often called shadowgraphs, have been an integral part of industrial NDE for decades. Their disadvantage is that depth information is lost; a three-dimensional (3-D) object is projected onto two-dimensions, i.e., onto a plane. Associated with this, a small defect can be difficult to resolve in standard radiography, since it contributes to the transmission measurement in the ratio of its linear dimension to the depth of the material along the transmission direction. It should, therefore, be of considerable economic interest to develop techniques which combine the transmission measurements from different viewing angles to obtain a three-dimensional, well resolved image of the object being evaluated.

The purpose of this paper is to describe two image reconstruction algorithms which are applicable to this general problem of reconstructing a 3-D object from a set of radiographic measurements. Image reconstruction techniques have been discussed extensively in the literature, and yet there has been relatively minor treatment of the case that the measurements are made in a truly three-dimensional arrangement around the object being evaluated. Rather, the measurements are typically made in sets of separate planes intersecting a 3-D object. The object is then reconstructed by obtaining the reconstruction of each plane separately, after which the planes are stacked together to obtain the 3-D result.* The main reason for the interest in a true 3-D measurement arrangement is that it should be possible to develop an efficient real-time system for the determination of defects.

After carrying out the image reconstruction, the problem still remains of identifying the defects which may be in the object. A defect must be classified, and there will usually be a set of accept-reject criteria which depends on the type of defect, taking into account the specific application of the object under evaluation. The accept-reject criteria must be analyzed from a statistical standpoint, and methods of statistical hypothesis testing are appropriate. Some of the main ideas in this approach are indicated in the last section of the paper.

IMAGE RECONSTRUCTION

As pointed out in the introduction, the bulk of the work in image reconstruction has involved measurements which are line integrals (designated projections) through a 2-D density $f(x,y)$.

The orientation of the line integral paths can be described in two geometries. In the early work sets of parallel ray projections through the density were utilized; projections in a given set are parallel to one another, but displaced in angle with respect to projections in the other sets. One such set of parallel ray projections is shown in Fig. 1(a). Reviews of a variety of reconstruction algorithms for the parallel ray geometry can be found in Refs. [4-7]. In some of the more recent work the sensors are arranged at fixed positions around the density to be reconstructed. A set of ray projections diverging from each source position is then utilized; this arrangement is shown in Fig. 1(b). Descriptions of the divergent ray (sometimes designated fan beam) reconstruction algorithms can be found in Refs. [8-10].

*This approach has also been used in using image reconstruction to determine stresses from ultrasonic measurements [2,3].

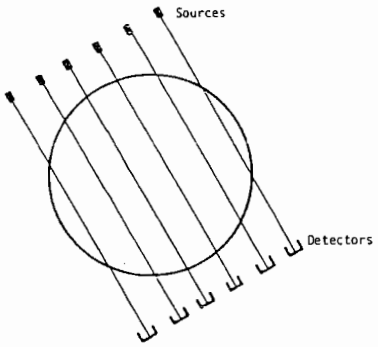

(a) Parallel Ray Geometry. One set of projections is shown; other sets cut through the density region at different angles.

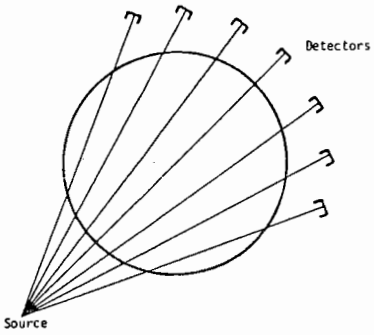

(b) Divergent Ray Geometry. One set of projections is shown; other sets emanate from other source locations around the density region.

Fig. 1 Measurement Geometries for Two-Dimensional Image Reconstruction

There are two principal methods which have been used to carry out the image reconstruction. The algebraic reconstruction techniques (ART) involve the inversion of a large matrix. They have the advantage that general density fields, even including spreading losses in the propagation of the signal to the detector, can be reconstructed. The convolution methods [11], on the other hand, are somewhat more restrictive but are usually an order of magnitude faster in computing time. This can be a significant difference if one is interested in developing real-time systems. It is the convolution approach which will be treated in this paper.

Both the 2-D parallel ray and the divergent ray reconstruction geometries of Fig. 1 have generalizations to three dimensions. The convolution solutions to the 3-D problem will be described next.

Reconstruction in 3-D From Parallel Rays - The basic equations for direct reconstruction from 3-D parallel ray projections were developed by Vainshtein and Orlov [12-14]. Their parameterization of the projections is convenient and, with minor modifications, is applicable to the divergent ray geometry also. With reference to Fig. 2, a ray is parameterized by the unit vector $\hat{\tau}$, as specified by the spherical coordinate angles (θ,ϕ), and a vector $\vec{\ell}$ lying in the plane perpendicular to $\hat{\tau}$ (denoted hereafter as the τ-plane).* The length $|\vec{\ell}|$ is the distance in the τ-plane from the ray to the origin. A convenient pair of orthogonal axes for decomposing $\vec{\ell}$ is given by

$$\hat{\ell}_{xy} \triangleq (\hat{\tau} \times \hat{k}) \,/\, (|\hat{\tau} \times \hat{k}|), \qquad \hat{\ell}_{z} \triangleq (\hat{\ell}_{xy} \times \hat{\tau}) \,/\, (|\hat{\ell}_{xy} \times \hat{\tau}|), \tag{1}$$

where $\hat{k}$ is the unit vector along the positive z axis. The ray is defined as the locus of points $\vec{\ell} + \tau\hat{\tau}$ as τ varies over $[-\infty,\infty]$. The parallel ray projections are thus given by

$$p(\vec{\ell},\hat{\tau}) = \int_{-\infty}^{\infty} f(\vec{\ell}+\tau\hat{\tau})d\tau \ , \tag{2}$$

where $f(\vec{x}) = f(x,y,z)$ is the density to be reconstructed. As seen in Fig. 2, the vector $\vec{\ell}$ is the projection of the sensor location onto the τ-plane. In a realistic arrangement it is assumed that the sensor is outside the region being measured; the actual sensor distance above the τ-plane (i.e., along the line $\vec{\ell} + \tau\hat{\tau}$) is not important due to Eq. (2). The reconstruction problem consists of determining $f(\vec{x})$ in Eq. (2), given all projections $p(\vec{\ell},\tau)$. The solution to this problem, as derived by Orlov [14], is

$$f(\vec{x}) = \frac{1}{4\pi^3} \int_0^{\pi} \sin\theta \, d\theta \int_0^{\pi} d\theta \iint_{-\infty}^{\infty} d\vec{\ell} \; p(\vec{\ell},\hat{\tau}) \, \varphi(\vec{x}_\tau - \vec{\ell}) \tag{3}$$

where $\vec{x}_\tau = \vec{x} - (\vec{x}\cdot\hat{\tau})\hat{\tau}$

and $$\varphi(\vec{x}_\tau - \vec{\ell}) = -\frac{1}{|\vec{x}_\tau - \vec{\ell}|^3} \qquad \vec{x}_\tau \neq \vec{\ell} \ .$$

Here the point to be reconstructed, $\vec{x}$, is projected onto the τ-plane (the latter defined by the angles θ and ϕ); the point $\vec{x}_\tau$ then enters in the argument of a convolving function φ. The $\vec{\ell}$-integration is the 2-D convolution of the projections $p(\vec{\ell},\hat{\tau})$ for each τ-plane with $\varphi(\vec{x}_\tau - \vec{\ell})$. After carrying out this convolution separately for each τ-plane, the contribution of each τ-plane is summed according to the angle integrations over θ and ϕ. The latter integrations are usually known as back-projections. It should be noted that in the solution form given in Eq. (3) we have neglected a contribution due to the singularity at $\vec{x}_\tau = \vec{\ell}$ which must be taken into account in a practical implementation. This contribution will be discussed later in the paper.

That Eq. (3) is actually a solution to the 3-D parallel ray reconstruction problem can be established by taking as the object density a 3-D Dirac delta function, and by verifying that Eq. (3) results in an output image which is, in fact, a delta function [14].

*Vectors will be denoted by an arrow, while the caret symbol designates a unit vector. The vector dot and cross product are denoted by "." and "×" respectively.

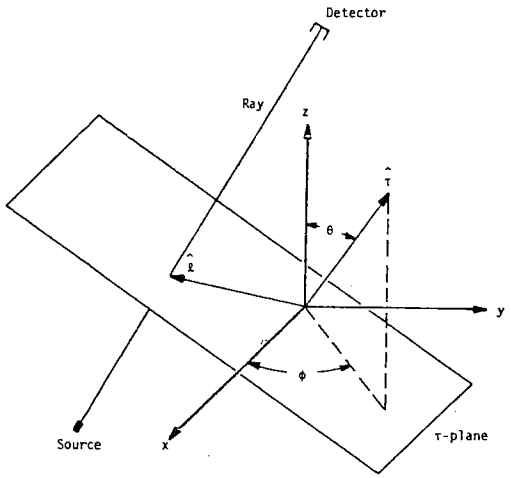

Fig. 2 Three-Dimensional Parallel Ray Geometry

Due to the structure of the solution in Eq. (3), a computer implementation is straightforward; in particular, an array processor can lead to extremely rapid computing times. In carrying out the implementation, a discrete form of the convolving function φ must be obtained. This involves a careful treatment of the singularity at $\vec{x}_\tau = \vec{\ell}$, as already indicated.

Reconstruction in 3-D From Divergent Rays - The measurement apparatus required for the above 3-D parallel ray reconstruction algorithm leads to some of the same difficulties that pertain in the 2-D case. For each set of parallel ray measurements, a series of translations of the source-detector combination is necessary. Following this, the entire apparatus must be rotated, after which the next set of parallel ray measurements is obtained, etc. This is difficult to achieve mechanically, especially if one is interested in a real-time imaging system. It is for this reason that the divergent ray reconstruction algorithm has found widespread application in the 2-D case, and similarly, the divergent ray geometry should be significant for the 3-D reconstruction problem. This problem, and its solution, will be discussed next.

The 3-D parallel ray parameterization shown in Fig. 2 can be modified for the case of the divergent ray projections. For this geometry, the sources are taken to lie on a sphere of radius D, with source coverage over the full solid angle. Referring to Fig. 3, $\hat{\ell}$ still lies in the τ-plane, but $\hat{\tau}$ now specifies the location of the source at $-D\hat{\tau}$. Varying $\vec{\ell}$ values now correspond to projections which scan the field in the angular variables.

The projections are given by

$$p(\vec{\ell},\hat{\tau}) = \int_{-\infty}^{\infty} f(\vec{\ell} + \tau'\hat{\tau}')d\tau' \quad , \tag{4}$$

where the direction of the ray is given by

$$\hat{\tau}' = \frac{D\hat{\tau} + \vec{\ell}}{\sqrt{D^2 + |\vec{\ell}|^2}} \quad . \tag{5}$$

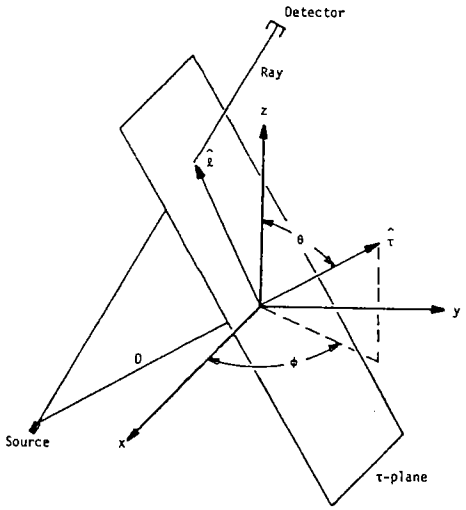

Fig. 3 Three-Dimensional Divergent Ray Geometry

The reconstruction problem is again to determine $f(\vec{x})$, given the projections $p(\vec{\ell},\hat{\tau})$. The solution to this inverse problem can be obtained by a direct transformation of the 3-D parallel ray solution in Eq. (3). The details are rather lengthy [15] and will be omitted here. The result is

$$f(\vec{x}) = \frac{1}{8\pi^3}\int_0^{\pi} d\theta \sin\theta \int_0^{2\pi} d\phi \frac{D^3}{(D+\vec{x}\cdot\hat{\tau})^3} \int_{-\infty}^{\infty}\int_{-\infty}^{\infty} d\ell_{xy}\, d \cdot \frac{Dp(\vec{\ell},\hat{\tau})}{\sqrt{D^2+|\vec{\ell}|^2}}\, \varphi(\vec{x}_\tau,\vec{\ell}) \tag{6}$$

where $\vec{x}_\tau \triangleq \frac{D}{D+\vec{x}\cdot\hat{\tau}} [\vec{x} - (\vec{x}\cdot\hat{\tau})\hat{\tau}]$,

and $\varphi(\vec{x}_\tau,\vec{\ell}) = -|\vec{x}_\tau - \vec{\ell} - \vec{\ell}\times\vec{x}_\tau/D|^{-3}$,

with $\vec{x}_\tau \neq \vec{\ell}$.

The reconstruction algorithm, Eq. (6) is similar to a convolve-and-backproject solution. However, because of the extra term $\vec{\ell}\times\vec{x}_\tau/D$, the inner integral over $\vec{\ell}$ is not a convolution integral. Thus, an exact implementation of Eq. (6) requires that the integrals be evaluated for each point $\vec{x}_\tau$ in the τ-plane. This would require a somewhat heavier computational burden than a true convolve-and-backproject solution.

In many experimental arrangements the cross product term can be neglected. To motivate this approximation, we note that the extra term $\vec{\ell}\times\vec{x}_\tau/D$ is relatively small if the source distance D is large compared to the distances $|\vec{x}_\tau|$ or $|\vec{\ell}|$. In a practical arrangement the sources would be outside of the volume to be reconstructed, so the values $|\vec{\ell}|$ and $|\vec{x}_\tau|$ would be smaller than D. The contribution of the cross product to the function φ is only of order $|\vec{\ell}|\ |\vec{x}_\tau|/D^2$ with respect to the contribution due to the vector $\vec{x}_\tau - \vec{\ell}$; this follows from noting that the cross product is orthogonal to $\vec{x}_\tau$ and $\vec{\ell}$, which allows φ for this case to be written as

$$\varphi = -\left\{|\vec{x}_\tau - \vec{\ell}|^2 + |\vec{\ell} \times \vec{x}_\tau|^2/D^2\right\}^{-3/2}$$

This function is singular at $\vec{\ell}=\vec{x}_\tau$, as suggested by looking at only the first term above; the added cross product term does not alter the position of the singularity. When the cross product term is neglected as an approximation, then the φ for this 3-D divergent ray solution becomes identical to that of the 3-D parallel ray case; it can then be implemented fairly easily.

Discrete Versions of the 3-D Solutions - The previous discussion applies when there is a continuum of sensors located around the region to be reconstructed, and when there is only a finite number of sensors and measurements per sensor. Assume that there are N sensors with location as given by the unit vector $\tau_i=(\theta_i,\phi_i)$, where the N angle pairs have some arbitrary distribution over the solid angle sphere. A discrete form of the backproject integral, the (θ,ϕ) integrations, is straight-forward to develop; it involves an appropriate weighted sum over the N sensor contributions.

On the other hand the discretized version of the convolving function φ appearing in the inner integrals requires more careful treatment, due to the singularity. To derive the result, we note that the exact convolving function is the result of a limiting process. It can be shown [15] that the convolving function, φ_ε, is given by

$$\varphi_\varepsilon = \begin{cases} \dfrac{2}{\varepsilon^3} & , \ |\vec{x}_\tau - \vec{\ell}| < \varepsilon \\ \dfrac{-1}{|\vec{x}_\tau - \vec{\ell}|^3} & , \ |\vec{x}_\tau - \vec{\ell}| \geq \varepsilon \ , \end{cases} \tag{7}$$

where φ_ε satisfies the equation

$$\iint d\vec{\ell} \ \varphi_\varepsilon(\vec{x}_\tau - \vec{\ell}) = 0, \text{ for all } \vec{x}_\tau \ . \tag{8}$$

In numerical approximations to φ_ε, the components of $\vec{\ell}$ take on a set of discrete values. On a cartesian grid φ has the form, for example,

$$\varphi(m\Delta\ell_{xy}, n\Delta\ell_z) = \frac{-w(m,n)}{[m^2\Delta\ell_{xy}^2 + n^2\Delta\ell_z^2]^{3/2}} \ , \text{ for}$$

$$|m| + |n| \neq 0 \ , \tag{9}$$

$$\varphi(0,0) = -\sum_{m,n} \varphi(m\Delta\ell_{xy}, n\Delta\ell_z)$$

$$|m| + |n| \neq 0 \ .$$

The coefficient $\varphi(0,0)$ is determined in accordance with Eq. (8).

The coefficients w(m,n) are typically of order 1 and were discussed in connection with the analogous 2-D problem in [16]. To each choice of coefficients w(m,n) corresponds a particular numerical integration procedure for the integral representation of $f(\vec{x})$.

One obvious choice for w(m,n) is simply unity for all m and n. In this case the convolving function in Eq. (9) is

$$\varphi(m,n) = -\frac{1}{\Delta^3} \ \frac{1}{[m^2+n^2]^{3/2}} \ , \tag{10a}$$

$$\text{for } |m| + |n| \neq 0$$

where for simplicity both quantization lengths $\Delta\ell_{xy}$ and $\Delta\ell_z$ have been assumed identical:

$$\Delta \triangleq \Delta\ell_{xy} = \Delta\ell_z \ .$$

The exact value of $\varphi(0,0)$ must be determined numerically, using Eq. (9); it can be shown through use of the Euler-Maclaurin summation formula to be approximately given by

$$\varphi(0,0) \cong \left[\frac{2\pi^2}{3} + 2\,\zeta(3)\right] / \Delta^3 \ , \tag{10b}$$

with $\zeta(\cdot)$ being the Riemann-Zeta function.

The above convolving function is only one of several possible ones that could be developed. Any discrete, well-behaved convolving function for this problem has the property that it involves a band-limiting approximation. In other words, a reconstruction according to Eq. (3) or Eq. (6), using the convolving function Eq. (10), is only accurate out to spatial frequencies of order $\omega \approx 1/\Delta$.

DEFECT DETERMINATION

Whether by solving the 3-D inverse problem using image reconstruction or by any other method, the result is a 3-D matrix of values corresponding to the observable being reconstructed, the density in the present case. In searching for defects, all the density values must be tested for deviations away from "normality." There is, of course, not a sharp division between normality and abnormality; the division depends upon the level of statistical error that can be tolerated in searching for the defects.

The simplest scheme for detecting the defects is to test each cell, or value of the 3-D matrix, in isolation from the other cells. Each cell can be examined in a binary hypothesis testing framework where the measured density is tested for belonging to one of two classes H_0: normal and H_1: abnormal. A simple Bayesian, Minimax [17] threshold may be set which distinguishes between the two classes.

The meaning of this test for the case of a defect consisting of a void in the material is sketched in Fig. 4. Here any density value greater than the indicated threshold T is declared normal, while any cell with density less than T is presumed to correspond to a void in the material; the cell is then declared abnormal. The density values for each hypothesis have a range as described by probability distributions. It is important to note that the two probability distributions invariably overlap in a practical system. Given the threshold setting, there is then a probability of detection P_D corresponding to hypothesis H_1: defect present, and a probability of false alarm P_{FA} corresponding to

the hypothesis H_0: cell normal, but with a defect nevertheless declared.

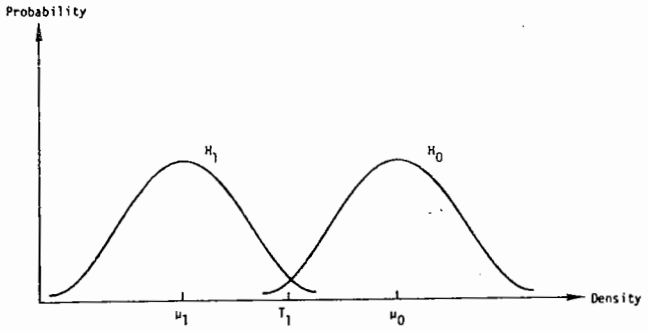

Fig. 4 Density Distributions for the two Hypotheses H_0: normal and H_1: abnormal

Depending on the resolution of the 3-D image that is actually achieved, the effect of a defect on the density will be somewhat reduced by an average over the cell volume. It will often be the case that the above test for an isolated cell does not then quite result in a threshold crossing for the outright classification as abnormal. Such cells must be evaluated in the context of the neighboring cell values. A number of classification procedures can be developed to treat this situation, to provide a more general and robust test than the simple binary hypothesis test. Several possible procedures will be described below.

To flag a cell that is marginal, a second threshold must be introduced. The second threshold can be set using the same Bayesian or Minimax criterion, but with a higher probability of false alarm. All marginal cells flagged in this manner constitute the input to the next stage of the detection process. Prior to the declaration of any region containing one of these cells as a flaw, on associative test procedure must be followed. One such associative measure is the volume of the connected region declared marginal. The connectedness can be tested using a minimal-spanning-tree algorithm [18] with a threshold on the maximum length between nodes. There are other measures for connectedness using clustering algorithms that have been used extensively in the literature [18].

The volume of the suspected region is a simple measure of the severity of the defect; the larger the volume, the more severe the defect. However, since the severity of any cell's variation is not taken into account, the measure lacks robustness. To improve on this, the volume can be weighted by the deviations of the questionable cell densities from the surrounding mean. If the region being tested has a mean μ, then the weighted volume V of the connected marginal cells with density values f_i and volumes v_i can be defined to be

$$V = \sum_i v_i |f_i - \mu| \quad .$$

The weighted volume measure V can then be used in a binary hypothesis test. The measure V has the properties of being translation and rotation invariant, as well as contrast independent.

However, this one-dimensional volume (weighted or unweighted) measure may not be enough, for some applications, to fully categorize the acceptability of the material. There are other multidimensional measures that take into account not only the size, but also the shape and distribution of the intensities. These measures are also invariant under rotation, translation and change in contrast [19]. These n-measures can then be tested [20] under the same H_0, H_1 hypotheses with the exception that the decision surface is then multidimensional. The number of dimensions that can be analyzed depends on how many statistical samples can be gathered prior to testing. The advantages to be gained from a multidimensional hypothesis testing is that, in the limit, one can use all the information embodied in the reconstructed image intensities.

CONCLUSION

The main purpose of this paper was to describe two direct 3-D image reconstruction algorithms involving a convolve-and-backproject approach. One of these, the 3-D divergent ray reconstruction algorithm, could be useful in radiographic NDE, in that it is amenable to a real-time implementation.

In addition, the statistical aspects of acceptance-rejection criteria were described. Several possible tests for defects were presented.

REFERENCES

1. See, for example, "Proceedings of the ARPA/AFML Review of Progress in Quantitative Nondestructive Evaluation," Third Annual Report, AFML-TR-78-55, under Contract F33615-74-C-5180, May 1978.

2. B.P. Hildebrand and D.E. Hufferd, "Mapping Residual Stress Fields by Ultrasonic Tomography," ibid., pp. 131-136.

3. J.D. Young and F.L. Lederman, "Quantitative Ultrasonic Tomographic Imaging," ibid., pp. 137-140.

4. Special Issue on Physical and Computational Aspects of 3-Dimensional Image Reconstruction, IEEE Trans. on Nucl. Sci., Vol. NS-21, No. 3, June 1974.

5. R.A. Brooks and G. DiChiro, "Principles of Computer Assisted Tomography (CAT) in Radiographic and Radioisotopic Imaging," Phys. Med. Biol., Vol. 21, No. 5, pp. 689-732, September 1976.

6. R.M. Mersereau and A.V. Oppenheim, "Digital Reconstruction of Multi-Dimensional Signals from Their Projections," Proc. IEEE, Vol. 62, No. 10, pp. 1319-1338, October 1974.

7. R. Gordon and G.T. Herman, "Three-Dimensional Reconstruction from Projections: A Review of Algorithms," Int. Rev. Cytol., Vol. 38, pp. 111-151, 1974.

8. G.T. Herman, A.V. Lakshminarayanan and A. Naparstek, "Convolution Reconstruction Techniques for Divergent Beams," Comput. Bio. Med., Vol. 6, pp. 259-271, 1976.

9. J.W. Beattie, "Tomographic Reconstruction from Fan Beam Geometry Using Radon's Integration Method," IEEE Trans. on Nucl. Sci., Vol. NS-22, pp. 359-363, 1975.

10. Z.H. Cho and J.K. Chan, "A Comparative Study of 3-D Image Reconstruction Algorithms with Reference to Number of Projections and Noise Filtering," IEEE Trans. on Nucl. Sci., Vol. NS-22, pp. 344-358, 1975.

11. G.N. Ramachandran and A.V. Lakshminarayanan, "Three-Dimensional Reconstruction from Radiographs and Electron Micrographs: Application of Convolution Instead of Fourier Transforms," Proc. Nat. Acad. Sci. U.S., Vol. 68, pp. 2236-2240, 1971.

12. B.K. Vainshtein and S.S. Orlov, "Theory of the Recovery of Functions from Their Projections," Soviet Physics-Crystallography, Vol. 17, No. 2, pp. 213-216, September-October 1972.

13. S.S. Orlov, "Theory of Three-Dimensional Reconstruction: I, Conditions for a Complete Set of Projections," Sov. Physics-Crystallography, Vol. 20, No. 3, pp. 312-314, May-June 1975.

14. S.S. Orlov, "Theory of Three-Dimensional Reconstruction: II, The Recovery Operator," Sov. Physics-Crystallography, Vol. 20, No. 4, pp, 701-709, July-August 1975.

15. R.V. Denton, B. Friedlander, and A.J. Rockmore, "Direct Three-Dimensional Image Reconstruction from Divergent Rays, to be published in IEEE Trans. on Nuc. Sci.

16. B.K.P Horn, "Density Reconstruction Using Arbitrary Ray-Sampling Schemes," Proc. IEEE, Vol. 66, No. 5, pp. 551-562, May 1978.

17. S. Zacks, The Theory of Statistical Inference, John Wiley, 1971.

18. R.O. Duda and P.E. Hart, Pattern Classification and Scene Analysis, John Wiley, 1973.

19. Sidhartha Maitra, "Moment Invariants," Proc. IEEE, Vol. 67, No. 4, pp. 697-699, April 1979.

20. A.K. Jain and W.G. Waller, "On the Optimal Number of Features in the Classification of of Multivariate Gaussian Data," Pattern Recognition, Vol. 10, No. 5/6, 1978.

SUMMARY DISCUSSION
(R. V. Denton)

Norman Bleistein (Denver Applied Analytics): I would like to make a suggestion as to why that cross product doesn't matter that much. If you look back in Fourier space, you're merely using high-frequency data. The point is, for high-frequency data the stationary phase contribution is the region where X and L are parallel. But that part vanishes due to the cross product.

R. Denton: I tend to agree with that.

# #